Diamond & Related Materials 89 (2018) 190–196

Contents lists available at ScienceDirect

Diamond & Related Materials

journal homepage: www.elsevier.com/locate/diamond

Tunable coloration of diamond films by encapsulation of plasmonic Ag nanoparticles

Shuo Li, Jason Bandy, Robert J. Hamers*

Department of Chemistry, University of Wisconsin-Madison, 1101 University Avenue, Madison, WI 53706, United States of America

ARTICLE INFO

Keywords:
Absorption
Optical properties characterization
Optical properties
Coatings
Windows
Plasma CVD
Diamond film

ABSTRACT

Chemical vapor deposition (CVD) grown diamond films are widely used as coating materials. While diamond thin films are typically clear or slightly gray in color, we demonstrate that diamond films of different optical properties and exhibiting different colors can be prepared by embedding Ag nanoparticles into the diamond film. Microwave plasma heating of Ag thin films deposited onto H-terminated diamond films grown on transparent fused quartz substrates leads to de-wetting and formation of a high density, two-dimensional array of size-controlled Ag nanoparticles. Surprisingly, scanning electron microscopy and transmission electron microscopy show that starting with Ag films < 30 nm diameter, dewetting and subsequent growth of a second diamond layer encapsulates the Ag nanoparticles, forming dense 2-dimensional arrays of diamond-encapsulated Ag nanoparticles. Under conditions used here, initial Ag films > 30 nm thickness lead to more polydisperse nanoparticles and the formation of Ag/diamond core/shell structures. By changing the thickness of the deposited Ag layer, the Ag nanoparticle size distribution can be changed, leading to changes in optical properties. Three-dimensional electromagnetic field modeling was performed for SiO_2-diamond/Ag/diamond-air structures produced by de-wetting of 20 nm thick Ag films show good qualitative agreement with experimental spectra.

1. Introduction

Diamond is well known for its extreme chemical stability, mechanical robustness, and combination of high index of refraction with high optical dispersion [1]. While diamond is typically transparent, from the ultraviolet through the infrared (approximately 215 nm through 4 μm wavelength), it has long been known that visible colors can be introduced into bulk diamond by introduction of defects [2] or by incorporation of impurities such as nitrogen or boron [3–5]. Yet, these methods are not readily applied to fabrication of deeply colored diamond thin films. Small metallic nanoparticles (NPs) frequently exhibit plasmonic effects that arise from the interactions between incident electromagnetic field and free electrons in the metal [6–9]. These plasmonic effects are manifest as wavelength-dependent changes in the optical response, leading to wavelength-dependent scattering and absorption. By tuning the size, shape, and composition of the nanoparticles, the optical response of materials incorporating plasmonic nanoparticles can be tuned across the spectrum [10–12]. Therefore, incorporating plasmonic metal particles into diamond films represents a promising approach to control the optical properties of diamond thin-film coatings [13].

While a number of metals exhibit plasmonic resonances, silver is particularly attractive because silver's plasmon resonances lie within the visible range (e.g., 400–700 nm) and are particularly strong due of silver's free-electron-like properties [8,9]. However, incorporation of silver into diamond is complicated by the fact that diffusion of silver is typically rapid at temperatures of diamond growth, which are typically > 700 °C [1]. For example, previous studies showed that Ag nanoparticles exhibited rapid coarsening on TiO_2 surfaces above 500 °C [14], on SiO_2 above 400 °C [15], and on polymer films above 300 °C [16]. A number of studies have investigated films of diamond-like carbon (DLC) with embedded Ag, typically made by sputtering methods [17–20]. In addition to exhibiting rapid coarsening at temperatures above ~300 °C [21], the optical properties of Ag-DLC films are generally dominated by the strong absorption within DLC due to π-π* transitions [21–28], yielding optical extinction constant k ranging from ~0.2 to 0.8 in the visible region of the spectrum [20,29,30]. In contrast, k for diamond thin films via plasma-enhanced chemical vapor deposition is ~0.02, a factor of 10 lower [31], and k for single-crystal diamond is nearly zero in the 400–700 nm spectral region [32]. Thus, incorporation of Ag nanoparticles into diamond should alter the diamond film's optical properties in a way that can be controlled through changes to the size and spatial distribution of the nanoparticles. Indeed, Shen and co-workers recently demonstrated formation of Ag nanoparticles

* Corresponding author.
E-mail address: rjhamers@wisc.edu (R.J. Hamers).

https://doi.org/10.1016/j.diamond.2018.09.003
Received 27 April 2018; Received in revised form 3 September 2018; Accepted 5 September 2018
Available online 06 September 2018
0925-9635/ © 2018 Elsevier B.V. All rights reserved.

within diamond by ion implantation of diamond substrates with 80 keV Ag^+ ions and observed evidence for plasmonic features in the optical spectrum [28]. Yet, high-energy ion implantation can also induce graphitization of the films and may not be easily replicated in many laboratories.

Here we demonstrate a convenient approach to forming diamond films with tunable optical properties by embedding two-dimensional arrays Ag nanoparticles into diamond films grown by plasma-enhanced chemical vapor deposition. We show that high-density Ag nanoparticle films with tunable nanoparticle size distributions can be formed by simple de-wetting of Ag films of specific thickness from H-terminated diamond samples in a hydrogen microwave plasma. Subsequent growth of diamond by introduction of small amounts of methane into the same microwave system leads to complete encapsulation of the nanoparticles into the growing diamond film. When starting with Ag layers 20 nm and below, the nanoparticles form a two-dimensional layer of closely coupled Ag nanoparticles. By controlling the thickness of the initial Ag film, we demonstrate the ability to alter the average nanoparticle size and the optical properties of the diamond film, as evidenced by UV–visible absorption spectra and direct visual observation of the diamond films. As proof-of-concept, we demonstrate that electromagnetic field modeling of the full three-dimensional SiO_2-diamond/Ag/diamond-air system yields results in good agreement with experiments, for NPs produced by dewetting from 20 nm Ag films. An important difference between the present work and most previous work incorporating nanoparticles into dielectric media is that the method described here confines the embedded nanoparticles into a nearly 2-dimensional array, leading to strong electromagnetic coupling between adjacent nanoparticles. The use of plasmonic effects to control optical properties of diamond films represents a potentially versatile approach to making films with novel optical properties.

2. Materials and methods

2.1. Growth of colored diamond-Ag-diamond films

Detonation nanodiamond with a nominal 4–10 nm size distribution (Nanoscale and Amorphous Materials, Inc.) was hydrogen-terminated by heating in a fused silica tube in a Thermolyne tube furnace for 5 h in a pure H_2 (> 99.999%, Airgas) atmosphere at 500 °C. The H-terminated powder was then sonicated in ethanol for 4 h and centrifuged for 15 min at 14,500 rotations per minute. The supernatant was used as a seeding solution. Dynamic light-scattering measurements (Malvern Zetasizer Nano) showed the diamond seeds to have an average hydrodynamic diameter of 35.2 nm, as shown in Supporting Information Fig. S1. Zeta-potential measurements measured in the same instrumented yielded $\zeta = +46.0$ mV. The concentration of the seeding solution was determined by direct weighing to be 385 mg/ml.

Fused quartz substrates (Ted Pella, Inc.) were cut into 1×1 cm^2 pieces and cleaned by sonication with acetone and water for 10 min respectively. To seed the diamond samples a 1 ml aliquot of the nanodiamond suspension in ethanol was spin-coated (3000 rpm, 30 s) onto the substrate. The positively charged nanodiamond particles are attracted electrostatically to the quartz substrate, while subsequent layers are repelled, leading to a monolayer film of diamond nanoparticles. Diamond thin films were grown using microwave plasma enhanced chemical vapor deposition (PECVD) in an AsTEX SDS 5010 Reactor that was modified in-house to provide additional sample heating capability and a thermocouple immediately below the substrate. Diamond films were grown using 200 standard cubic centimeters per minute (sccm) H_2 and 3 sccm CH_4 at a power of 800 W (temperature = 575 °C), with a constant total pressure of 48 Torr. The first diamond layer was grown for 15 min and was then quickly transferred through air (typically air exposure < 3 min) to an electron-beam metal evaporator, where Ag films with different thicknesses were deposited at a rate of 0.1 Å/s. Films of 10, 20, and 50 nm thickness are reported in this manuscript. After Ag film growth, the samples were again transferred quickly (< 3 min) back into the diamond PECVD system and exposed to a H_2 plasma to dewet the thin film and form a dense array of Ag nanoparticles. While varying times and power levels were explored, samples shown here were dewetted using 600 W (temperature 500 °C) and a time of 10 min. To encapsulate the Ag NPs, the dewetted Ag-diamond sample was seeded again with nanodiamond suspension, and a second diamond layer on the sample was immediately grown, using 200 sccm H_2 and 3 sccm CH_4 (total pressure 48 Torr) at a power of 800 W, typically for 15 min. The sample temperature during growth was approximately 575 °C. In some cases, samples were removed at various stages of this procedure to characterize the size, shape, and other properties of the films.

2.2. Diamond film characterization

Scanning electron microscopy (SEM) and Energy-Dispersive X-Ray Spectroscopy (EDS) measurements were carried out using a Leo Gemini Supra 55 VP field-emission scanning electron microscope. To best capture the film morphology, an SE2 detector was used for imaging. Energy dispersive X-ray spectra were obtained on this same instrument using a ThermoFisher UltraDry Compact EDS detector. Transmission electron microscopy (TEM) characterization was performed using a Tecnai TF-30 microscope operating at accelerating voltage of 300.0 kV. Raman spectra were obtained in a confocal geometry using a LabRam Aramis Confocal Raman Microscope with excitation at 442 nm. Optical transmission spectra of the samples were collected using Shimadzu 2401PC double-beam ultraviolet–visible spectrophotometer.

3. Results and discussion

We first characterized the diamond film embedded with Ag NPs at different growth stages of preparation using SEM. As shown in Fig. 1a, the initial diamond layer grown on fused silica is composed of crystallites with typical facet sizes of 100–200 nm. Fig. 1b shows the surface morphology after a 20 nm thick Ag film was deposited on the sample, transferred back to the PECVD chamber, and exposed to a H_2 plasma for 10 min. In Fig. 1b it is clear that the Ag film de-wetted into finely dispersed, approximately spherical Ag NPs with diameters ranging from 10 to 40 nm, while the diamond in regions surrounding the Ag NPs maintains its original morphology. Fig. 1c shows an SEM image after another layer of diamond was grown on the de-wetted Ag NP layer, thereby forming a SiO_2-diamond-Ag-diamond structure in which the Ag nanoparticles are completely encapsulated and therefore protected from external chemical or mechanical impacts. Fig. S2 (Supplemental Information) shows a cross-sectional SEM image of a diamond film grown on quartz for 30 min, demonstrating a thickness of 250 nm, representing a growth rate of approximately 8 nm/min.

To show that the resulting structures have Ag *within* the diamond layers but not on the topmost surface, we used energy-dispersive X-ray spectroscopy (EDS) and X-ray photoelectron spectroscopy (XPS). Fig. S3 (Supporting Information) shows EDS spectra obtained using an electron acceleration voltage of 25 kV; in this case the x-ray emission is clearly detected, while a spatial map shows no detectable spatial variation, consistent with the limited spatial resolution of EDS and the close spacing between Ag NPs revealed in SEM. At lower electron acceleration voltages of 5 kV (Fig. S4, Supporting Information), no Ag X-ray emission was observed. Similarly, no Ag emission was observed from a control sample of diamond on quartz (S5, Supporting Information). To show that the Ag is not present at significant concentrations on top of the diamond surface after growth of the second diamond layer, we measured XPS spectra (Fig. S6, Supporting Information). In the XPS spectrum, no Ag signal can be detected, while the C(1s) peak shows a single narrow peak typical of diamond. The combination of EDS and XPS shows that Ag is present within the diamond film but is not present on the top surface.

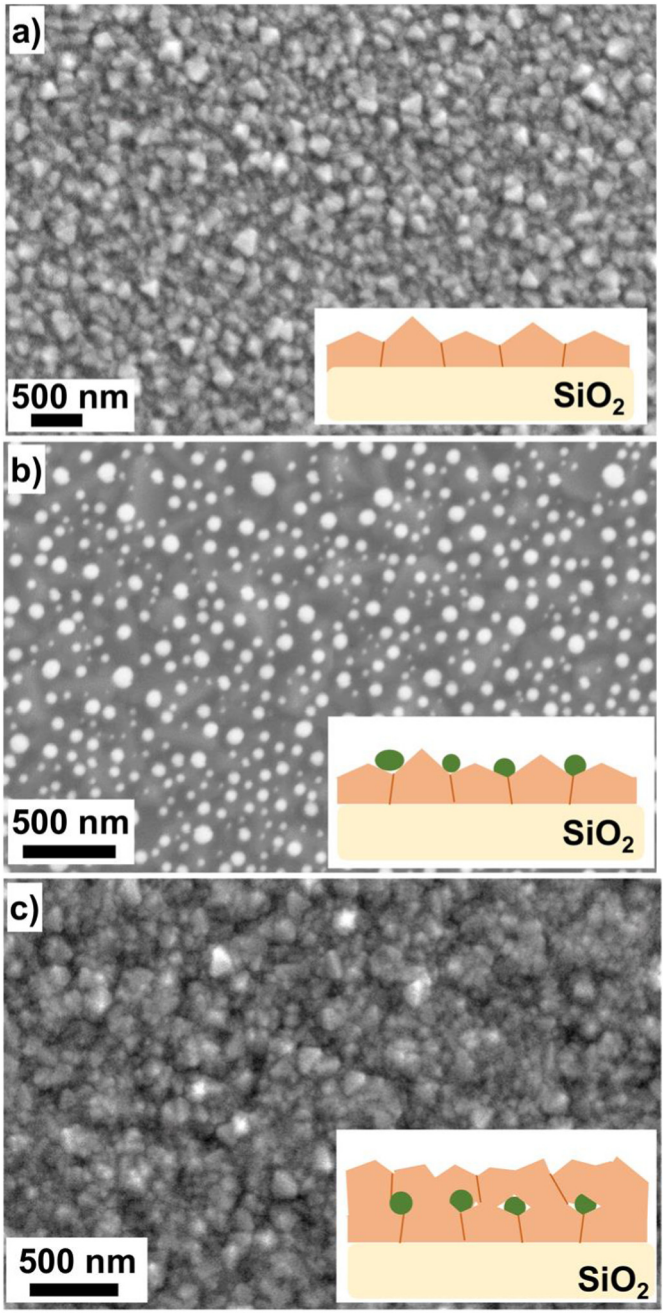

Fig. 1. Top-view SEM images and schematic illustrations (insets) of a) diamond grown on SiO_2; b) dewetted Ag nanoparticles on diamond/SiO_2; and c) film of Ag nanoparticles fully encapsulated by diamond.

The introduction of Ag alters the growth morphology and leads to some increased in graphitic carbon. Fig. S7 (Supporting Information) shows confocal Raman spectra of the initial diamond film and of the diamond-Ag-diamond composite structure. Both samples exhibit a sharp peak near 1330 cm^{-1}, close to the 1332 cm^{-1} diamond peak. In addition, broader peaks near 1370 and 1580 cm^{-1} are observed; these peaks are frequently attributed to the "D" and "G" bands of graphitic material, respectively [33]. Note that the cross-section for Raman scattering of sp^2-hybridized carbon is approximately 100 times higher than that for sp^3-hybridized diamond, therefore the diamond film has good diamond quality [34,35]. The D-Ag-D also has another peak at around 1150 cm^{-1}, which is reported as the nanocrystalline diamond peak [36,37].

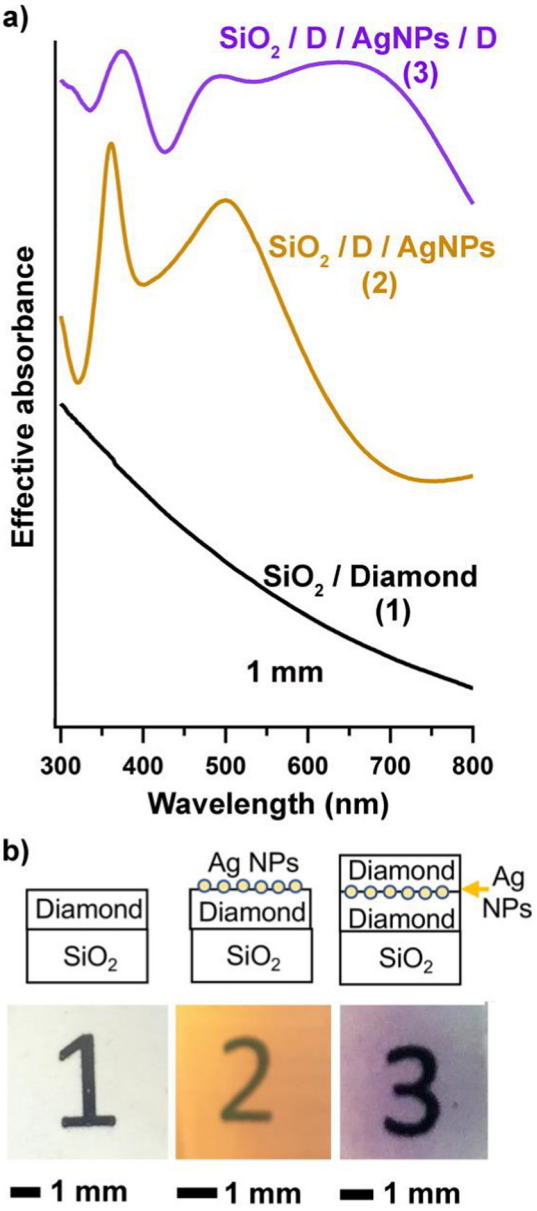

Fig. 2. Optical properties associated with incorporation of Ag nanoparticles into diamond film. a) Effective absorbance measured from 3 identical films at different stages of processing. b) White-light images of samples held above white paper with the corresponding digits "1", "2", and "3" on the paper. Samples were illuminated from above using ambient room lighting.

3.1. Optical properties of diamond films with embedded Ag nanoparticles

Fig. 2 shows optical absorption spectra (made in transmission mode) of three identical samples at different stages of processing, while Fig. 2b shows the corresponding white-light photographs of the samples when held above a white background with "1", "2", and "3" written on the paper. The absorption spectrum of pure diamond on fused silica (SiO_2) shows no obvious peaks across the UV to visible region with only a slow increase at shorter wavelengths due to the increased reflectivity. After deposition and dewetting of the Ag film, an obvious peak near 360 nm can be observed, along with a broader peak at 500 nm. After growth of the second diamond film, the spectrum is more complicated and shows peaks near 365, 500, and 650 nm. The absorption spectrum of sample (3) is qualitatively similar to that presented by Shen, et al. from diamond samples that were Ag^+-implanted and then annealed to form Ag nanoparticles [28]. Fig. 2 also shows photographs of the three

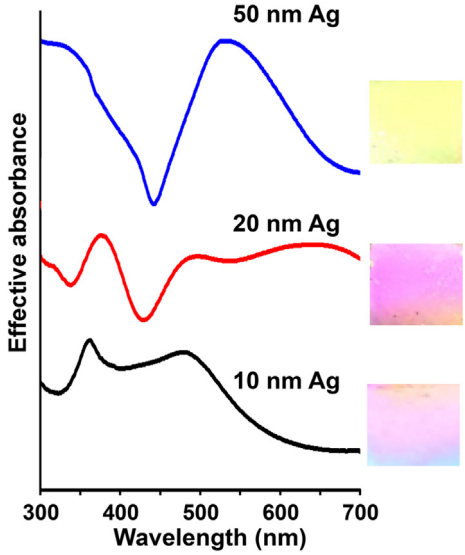

Fig. 3. UV–Vis spectra and corresponding white-light optical images of D-Ag-D on fused silica with 10, 20 and 50 nm initial Ag layer thicknesses.

samples held above a white background, illuminated from above. The diamond-on-quartz sample (1) is white, the de-wetted Ag nanoparticles on diamond (2) appears yellow, while the film with diamond-encapsulated Ag nanoparticles (3) appears reddish. In each case the films remain transparent, as text underneath the samples can be read clearly. This color change clearly demonstrates that incorporation of Ag nanoparticles into the films strongly affects the optical properties. As will be discussed below, the optical properties of the Ag-diamond composite films can be qualitative reproduced by full 3-dimensional modeling, but due to the close proximity of adjacent nanoparticles and the high index of refraction of diamond the detailed origin of the optical response cannot be attributed solely to the plasmonic features ascribed to individual isolated nanoparticles [38].

3.2. Control of optical properties by changing nanoparticle diameter

By varying the thickness of the deposited Ag film, the size distribution of the Ag nanoparticles can be varied. Fig. 3 shows optical transmission spectra of diamond-encapsulated Ag nanoparticles made starting with Ag films of 10, 20, and 50 nm thickness. With the 10 and 20 nm films, the feature near 365 nm wavelength is retained. The feature arising at 480 nm from dewetting of 10 nm Ag films shifts to slightly longer wavelength for thicker films. For 50 nm Ag dewetting as the Ag NPs became larger, the maximum extinction occurs at ~550 nm. Fig. 3 also shows the actual optical images of ~5 mm square regions, demonstrated changes in color as the nanoparticle size changes. Some lateral variations in occur, arising from changes in the temperature across the sample that in turn alters the size distribution of the nanoparticles and the associated color changes.

To better understand how different processing conditions alter than nanoparticle shape and spatial distribution, we used scanning electron microscopy and transmission electron microscopy to characterize the D-Ag-D composite films during initial stages of growth of the second diamond layer. SEM images of nanoparticle films made by dewetting of Ag films of different thickness are shown in Supporting Information Fig. S8, along with statistical distributions of particle sizes made by analyzing multiple SEM images. We also measured particle size distribution after growth of the diamond second layer. In this case after the second layer growth was completed (15 min), the composite films were fractured from the SiO_2 substrate to expose thin regions suitable for TEM imaging and particle size counting. Fig. 4 shows TEM images through the diamond-Ag-diamond layers, while Supporting Information Fig. S9

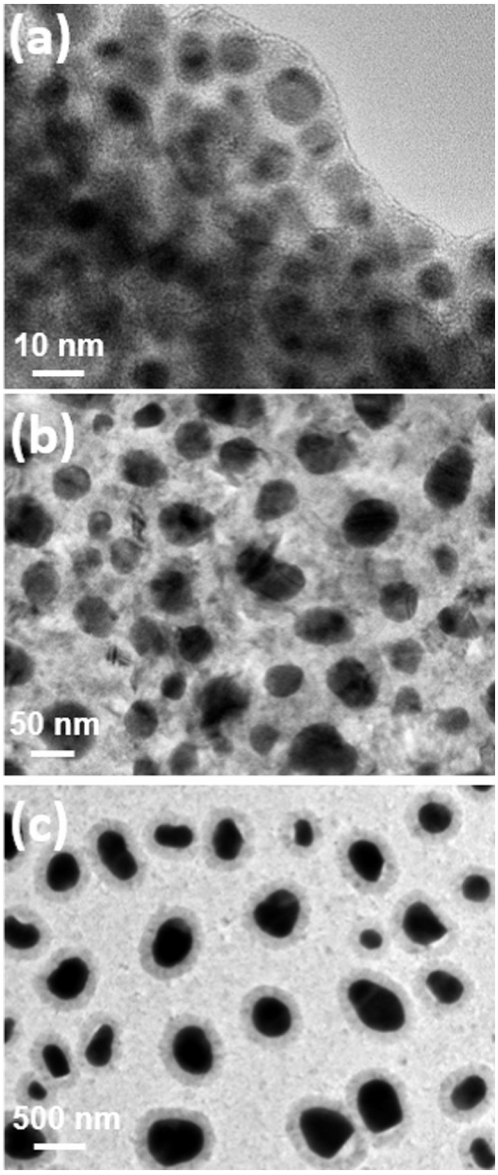

Fig. 4. TEM images of D-Ag-D samples prepared by depositing Ag layers of different thicknesses, dewetting, and growth of a second diamond layer for 15 min. a) 10 nm Ag thickness, b) 20 nm Ag thickness, and c) 50 nm Ag film thickness.

shows the distribution of particle sizes. The TEM image in Fig. 4a shows that starting with a 10 nm Ag film, after dewetting and encapsulation the diamond film has a very high density of embedded Ag NPs with diameters of 10–20 nm, corresponding well with the size-distribution results from the SEM images. Close examination shows lattice images in some of the Ag NPs. Starting with a thicker 20 nm Ag film, Fig. 4b shows embedded Ag nanoparticles with diameters of 20–50 nm. Close examination of images of smaller-sized nanoparticles, as in Fig. 4a and b, appear to show an abrupt interface from Ag to diamond, with no evidence for onion-like graphite nanoshells or other structures. Starting with a 50 nm Ag film, the TEM image in Fig. 4c shows formation of Ag NPs (frequently non-spherical) with diameters of 100–300 nm. The particle size distribution measurements (Supporting Information Fig. S9) shows that Ag films 10 nm thickness produce Ag nanoparticles 10 nm to 20 nm in diameter, and 20 nm Ag films produce nanoparticles primarily in the 20–50 nm size range. In both cases the nanoparticles are in close proximity to one another; as discussed later, this leads to electromagnetic coupling between the nanoparticles. As the initially

deposited layer thickness increases to 50 nm, the Ag nanoparticle diameters increase rapidly to 300–500 nm, forming larger, isolated nanoparticles. In this size regime, the particles also begin to exhibit some elongation.

While for small nanoparticles the TEM images appear to show NPs completely embedded into a diamond film for the largest particle sizes investigated the individual nanoparticles have a visible diamond shell grown around them, visible as a slightly darkened halo in Fig. 4c. The diamond shell is approximately 125 nm thick, corresponding to a growth rate of ~8 nm/min. This rate is the same as that observed for the initial diamond films grown on the quartz substrate shown in Supporting Information Fig. S1. Fig. S10 in Supporting Information shows a high-resolution TEM image of a single Ag nanoparticle with its diamond shell prepared like those in Fig. 4c. At this high resolution, the grain structure within the diamond layer can be partially resolved. [1,39–41] No indication of graphitic or other intermediate layers is observed.

To test whether the diamond shells observed in Figs. 4c and S10a are complete, we conducted studies in which we immersed such nanoparticle films into a boiling mixture of concentrated $H_2SO_4HNO_3/HClO_4$, 1:1:1 ratios by volume, for 24 h; this solution is expected to rapidly etch amorphous carbon and most other possible contaminants. Fig. S10b (Supporting Information) shows SEM images of the resulting film; the Ag core (which appears bright in SEM) and the diamond shell both appear to remain intact. Direct comparison of nanoparticle films before and after acid immersion show no significant change in the nanoparticles. These results strongly suggest that the shells visible in Fig. 4c are complete and are able to completely protect the encapsulated Ag nanoparticles.

Overall, our data show that samples starting with Ag layers < 30 nm in diameter lead to abrupt interfaces and dense arrays of diamond-embedded Ag nanoparticles. For samples with initial Ag layers > 50 nm in thickness, halting the growth of the diamond overcoat after 15 min shows nanoparticles with core-shell structures like those shown in Fig. 4c. Further studies show that when the second-layer growth is continued for a longer time, the core-shell structures visible in Fig. 4c merge into a continuous film resembling those in Fig. 4a and b. In addition, when growth of the second layer is halted after shorter periods of time, core-shell structures are also observed from 10 nm and 20 nm Ag films. From these studies, we conclude that the apparent transition from continuous film (Fig. 4a, b) to core-shell structure (Fig. 4c) simply reflects different stages in a common growth process. For all Ag thicknesses, growth of a second diamond layer shows core-shell structures at short growth times and a continuous film at longer growth times. We note that the thickness of the film observed on the Ag nanoparticles appears to correspond well to that expected from the from growth rate on the quartz substrate, as shown in Fig. S1.

3.3. Modeling of optical properties

The spectra and visible optical properties are clearly a result of the presence of nanoparticles within the diamond film. However, because of the close proximity of the nanoparticles, adjacent nanoparticles are electromagnetically coupled to one another. Furthermore, because of diamond's high index of refraction, the optical properties of the diamond-encapsulated Ag layers couple to interference effects within the diamond films. Consequently, the optical properties of the Ag-diamond composite films cannot be easily interpreted based on the commonly used theories of scattering from isolated nanoparticles. Nevertheless, Mie theory provides a useful starting point for understanding the response. Mie theory predicts for a single isolated nanoparticle embedded in a dielectric medium, the cross-section for scattering is given by [42,43].

$$E(\lambda) = \frac{24\pi^2 a^3 \epsilon_m^{3/2}}{\lambda ln(10)}\left[\frac{\epsilon_i(\lambda)}{(\epsilon_r(\lambda) + 2\epsilon_m(\lambda))^2 + \epsilon_i(\lambda)^2}\right] \quad (1)$$

where a is the nanoparticle radius, λ is the wavelength of light, ϵ_r and ϵ_i are the real and imaginary parts of the dielectric constant of the nanoparticle, and ϵ_m is the dielectric constant of the surrounding matrix (which is assumed to be lossless). The real (ϵ_r) and imaginary (ϵ_i) parts of the complex dielectric function are related to the index of refraction n and absorption coefficient k by $\epsilon_r = n^2 - k^2$ and $\epsilon_i = 2nk$. The factor in brackets resembles a Lorentzian-like function that reaches a maximum when $\epsilon_r(\lambda) + 2\epsilon_m(\lambda) = 0$. Based on published values of optical constants for Ag and for diamond, this simple equation predicts a resonance near 385 nm for Ag nanoparticles in air ($\epsilon_m = 1$), which shifts to 580 nm in (lossless) diamond ($n = 2.4$, $\epsilon_m = n^2 = 5.81$). However, for particles larger than ~20 nm diameter, additional quadrupolar and higher-order modes become important [44]. In our case, the close coupling of adjacent nanoparticles is important. Unlike the more common case of Ag nanoparticles embedded within films of diamond-like carbon [26,27,30,45,46], in our case the nanoparticles are confined to lie within a nearly two-dimensional layer, and Fig. 4a and b show that the nanoparticles are in close proximity to one another where electromagnetic coupling between nanoparticles becomes important. [47].

In order to understand the factors controlling the optical properties of the nanoparticle-embedded diamond films, we used finite element modeling as implemented in Comsol Multiphysics to obtain the full 3-dimensional solution to Maxwell's equations for air-diamond-SiO_2 structures in which Ag nanoparticles were embedded into the center of the diamond film. Because of the complexity of the geometry, we focus our attention on one size only, consisting of nanoparticle produced by dewetting of 20 nm thick Ag films and the formation of Ag nanoparticles 70 nm in diameter separated by 95 nm, yielding the same Ag coverage per unit area. We note that thicker Ag layers produced nanoparticle distributions that are more heterogeneous in size and shape (as shown in Fig. 4), while thinner layers have greater uncertainty in actual coverage making comparison with experiments more difficult. We therefore use 20 nm films to as a model system for analysis.

To simulate the fact that our nanoparticles are present in a nearly two-dimensional film, we use periodic boundary conditions, thereby accounting for electromagnetic coupling between adjacent nanoparticles. In addition, we used perfectly matched layers at the left and right boundaries (not shown in Fig. 5a) to eliminate spurious effects due to reflection from the back of the SiO_2 layer, while including interference effects at diamond-air and diamond-SiO_2 interface. These calculations include the wavelength-dependent index of refraction (n) and absorption constant (k) for silver [48,49] and diamond. For diamond, we explored both parametrized constants for single-crystal diamond and published data for CVD diamond films [31,50]. Yin, et al. reported values of n and k for a variety of diamond thin films produced by chemical vapor deposition under conditions similar to those used here; Yin's data show that n is nearly constant through the visible range, while k varies linearly with wavelength. Based on their data, we used a constant value of n = 2.13 and parameterized the values of k as $k(\lambda) = 0.042 - 5.17 \times 10^4(\lambda - 2.00 \times 10^{-7})$ where λ is the wavelength in meters [31].

Fig. 5 shows the results of example calculations for the effective absorbance as a function of wavelength for a variety of diamond-Ag structures, for a 35 nm radius nanoparticle embedded in the center of a 250 nm diamond film on SiO_2 substrate. The effective absorbance is extracted from the $A_{effective} = -log_{10}(|S_{21}|^2)$, where S_{21} is the S-parameter (scattering parameter) that describes transmission of electromagnetic energy through the sample.

Fig. 5 shows that for a 250 nm diamond film on SiO_2, interference effects are expected to induce small apparent absorbances near 350, 490, and 800 nm. A planar Ag film 25 nm in thickness embedded in the middle of a diamond film has a similar overall response, with the peak at 490 nm attenuated. In Fig. 5, traces labeled (3) and (4) show the predicted effective absorbance from 70 nm diameter Ag nanoparticles de-wetted from a 125 nm diamond film, differing in whether the Ag

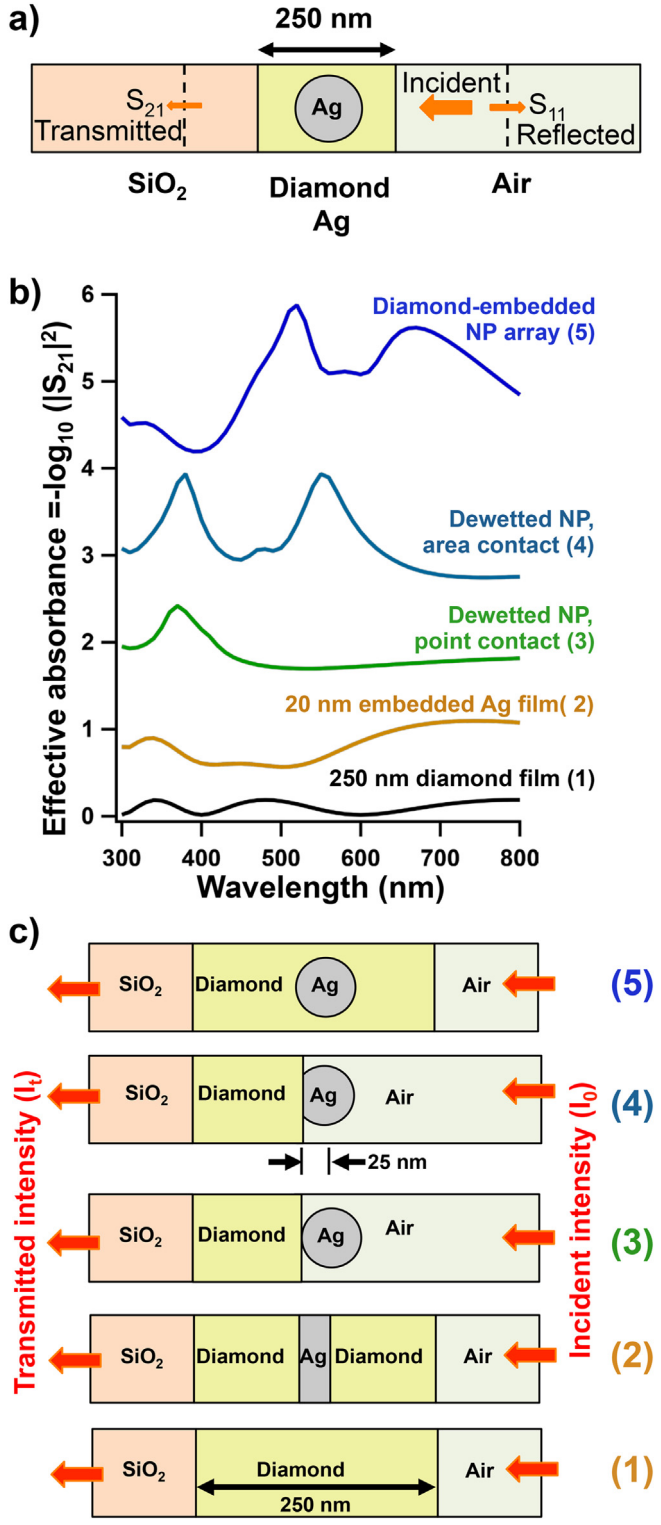

Fig. 5. Modeling results for 2-dimensional square array of Ag nanoparticles in diamond films. a) Overview of model used, b) effective absorbance calculated from full 3-dimensional solution of Maxwell's equations, c) corresponding physical geometries used a model inputs. Trace (2) represents a 25 nm Ag film embedded between two 125 nm diamond films. Traces (3–5) represent an infinite square array of 70 nm diameter nanoparticles separated by 95 nm. In trace (3), the 70 nm diameter Ag NP makes a point contact with the diamond film. In trace (4), the NP makes a contact at radius = 25 nm, placing 37% of surface area in contact with diamond. In all cases, 2-dimensional periodic boundary conditions were applied perpendicular to the interfaces.

nanoparticle makes a point contact (trace 3) or has a more significant contact area (trace 4). Perhaps not surprisingly, the Ag nanoparticle making only a point contact (trace 3) gives rise to a single peak at a frequency close to that of the dipolar mode of an isolated Ag nanoparticle in air (~385 nm) predicted from Mie theory, while the Ag nanoparticle making more direct contact with the underlying diamond film (trace 4) yields two features, one near 385 nm and one near 580 nm; the latter is similar to the expected Mie resonance frequency of a Ag nanoparticle embedded completely in diamond. A comparison of our measured absorption spectrum of Ag nanoparticles de-wetted from diamond but without second-layer diamond growth (Fig. 2a, trace 2) is quite similar to that in trace 4 of Fig. 5b.

In Fig. 5, trace 5 (labeled "Diamond-embedded NP array") shows the results of a calculation for two-dimensional array of 70 nm diameter nanoparticles separated by a mean distance of 85 nm. This trace simulates the result of dewetting a 25 nm Ag film into nanoparticles with the same total amount of Ag per unit area. For the two-dimensional array of nanoparticles, the spectrum is again dominated by two large features near 500 nm and 650 nm. These features are in good agreement with those observed from the Ag-embedded nanoparticles shown in Fig. 2, trace 3. The experimental spectrum also shows an additional feature near 365 that is typical of Ag in contact with air, suggesting that some nanoparticles may be on particle contact with diamond and in partial contact with air. Indeed, for large nanoparticles, the TEM images in Fig. 4c clearly show that some NPs have an apparent gap (visible as lighter region between the diamond shell and the dark NP core) visible, suggesting that some NPs embedded in the film may still have some direct contact with air.

While even a full two-dimensional model cannot be expected to accurately reproduce the experimental results due to the dispersion of sizes and nanoparticle separations and the presence of non-sphericity in the nanoparticles (visible in Fig. 4) [44,47,51], our results show that full 3-dimensional electromagnetic modeling is able to reproduce the qualitative features. Importantly, the presence of peaks in the optical absorption spectra in the range of 475–650 nm show that, in agreement with the TEM images, a large fraction of the nanoparticles persist as sub-100 nm nanoparticles. A full analysis of these 2-dimensional nanoparticle arrays would require electromagnetic modeling that incorporates heterogeneity of nanoparticle size, shape and separation. Nevertheless, when starting with thin films < 30 nm, the nanoparticles are approximately spherical in size and have a more uniform distribution of sizes that may provide the ability to confer useful optical properties into diamond films.

4. Conclusions

Our results demonstrate a new approach to preparation of densely colored diamond thin films by incorporating 2-dimensional arrays of Ag nanoparticles into the center of diamond thin film layers. While significant coarsening of nanoparticles might be expected under conditions of diamond growth, our results show that Ag nanoparticles produced on H-terminated diamond retain their small size sufficiently long to enable encapsulation of the nanoparticles into the growing diamond film. The optical properties clearly demonstrate plasmonic resonances and are qualitatively similar to those expected from full three-dimensional electromagnetic field modeling of two-dimensional arrays of Ag nanoparticles in diamond. While demonstrated here with a single layer of nanoparticles, it should be possible to make even more intensely colored films by repeated application. Additionally, greater control over the plasmonic features could be achieved using lithographic patterning techniques to achieve more homogeneous distribution of nanoparticle sizes and shapes, albeit in a less scalable manner. Nevertheless, the work reported here demonstrates that simple dewetting procedures provide a convenient method for imparting tunable color to diamond via encapsulation of Ag nanoparticles.

Acknowledgments

This work was supported by the National Science Foundation Division of Materials Research, DMR-1507432. S.L. acknowledges PPG Corporation for a PPG Summer Fellowship.

Appendix A. Supplementary data

Supplementary data to this article can be found online at https://doi.org/10.1016/j.diamond.2018.09.003.

References

[1] P.W. May, Diamond thin films: a 21st-century material, Philos. Trans. R. Soc. Lond. Ser. A Math. Phys. Eng. Sci. 358 (2000) 473–495.
[2] L.S. Hounsome, R. Jones, P.M. Martineau, D. Fisher, M.J. Shaw, P.R. Briddon, S. Oberg, Origin of brown coloration in diamond, Phys. Rev. B 73 (2006) 8.
[3] P. Sacerdote, Changes in coloration of diamonds under the effect of various physical agents, C. R. Hebd. Seances Acad. Sci. 149 (1909) 993–994.
[4] F. Jelezko, J. Wrachtrup, Single defect centres in diamond: a review, Phys. Status Solidi A Appl. Mater. 203 (2006) 3207–3225.
[5] F. De Weerdt, J. Van Royen, Defects in coloured natural diamonds, Diam. Relat. Mater. 10 (2001) 474–479.
[6] C.J. Murphy, T.K. Sau, A. Gole, C.J. Orendorff, Surfactant-directed synthesis and optical properties of one-dimensional plasmonic metallic nanostructures, MRS Bull. 30 (2005) 349–355.
[7] P.K. Jain, X.H. Huang, I.H. El-Sayed, M.A. El-Sayed, Noble metals on the nanoscale: optical and photothermal properties and some applications in imaging, sensing, biology, and medicine, Acc. Chem. Res. 41 (2008) 1578–1586.
[8] S.L. Zou, G.C. Schatz, Narrow plasmonic/photonic extinction and scattering line shapes for one and two dimensional silver nanoparticle arrays, J. Chem. Phys. 121 (2004) 12606–12612.
[9] H. Wang, D.W. Brandl, P. Nordlander, N.J. Halas, Plasmonic nanostructures: artificial molecules, Acc. Chem. Res. 40 (2007) 53–62.
[10] J.A. Schuller, E.S. Barnard, W. Cai, Y.C. Jun, J.S. White, M.L. Brongersma, Plasmonics for extreme light concentration and manipulation, Nat. Mater. 9 (2010) 193–204.
[11] S. Linic, P. Christopher, D.B. Ingram, Plasmonic-metal nanostructures for efficient conversion of solar to chemical energy, Nat. Mater. 10 (2011) 911–921.
[12] M.A. García, Surface plasmons in metallic nanoparticles: fundamentals and applications, J. Phys. D. Appl. Phys. 44 (2011) 283001.
[13] M. Rycenga, C.M. Cobley, J. Zeng, W. Li, C.H. Moran, Q. Zhang, D. Qin, Y. Xia, Controlling the synthesis and assembly of silver nanostructures for plasmonic applications, Chem. Rev. 111 (2011) 3669–3712.
[14] S. Moldovan, L. Roiban, D. Georgescu, L. Baia, O. Ersen, Thermal evolution of silver nanoparticles onto porous TiO_2 nanostructures, Catal. Today 284 (2017) 221–228.
[15] J.M. Sun, D. Ma, H. Zhang, X.M. Liu, X.W. Han, X.H. Bao, G. Weinberg, N. Pfander, D.S. Su, Toward monodispersed silver nanoparticles with unusual thermal stability, J. Am. Chem. Soc. 128 (2006) 15756–15764.
[16] J. Siegel, P. Jurik, Z. Kolska, V. Svorcik, Annealing of silver nanolayers sputtered on polytetrafluoroethylene, Surf. Interface Anal. 45 (2013) 1063–1066.
[17] Š. Meškinis, T. Tamulevičius, G. Niaura, K. Šlapikas, A. Vasiliauskas, O. Ulčinas, S. Tamulevičius, Surface enhanced Raman scattering effect in diamond like carbon films containing ag nanoparticles, J. Nanosci. Nanotechnol. 16 (2016) 10143–10151.
[18] C. Wang, X. Yu, M. Hua, Microstructure and mechanical properties of Ag-containing diamond-like carbon films in mid-frequency dual-magnetron sputtering, Appl. Surf. Sci. 256 (2009) 1431–1435.
[19] S. Tamulevičius, Š. Meškinis, M. Sigitas, T. Tamulevičius, H.-G. Rubahn, Diamond like carbon nanocomposites with embedded metallic nanoparticles, Rep. Prog. Phys. 81 (2018) 024501.
[20] D. Franta, L. Zajickova, I. Ohlidal, J. Janca, Optical characterization of diamond-like carbon films, Vacuum 61 (2001) 279–283.
[21] S. Meškinis, T. Tamulevičius, G. Niaura, K. Šlapikas, A. Vasiliauskas, O. Ulčinas, T. Tamulevičius, Annealing effects on structure and optical properties of diamond-like carbon films containing silver, Nanoscale Res. Lett. 11 (2016) 146.
[22] I. Yaremchuk, A. Tamuleviciene, T. Tamulevicius, K. Slapikas, Z. Balevicius, S. Tamulevicius, Modeling of the plasmonic properties of DLC-Ag nanocomposite films, Phys. Status Solidi A Appl. Mater. 211 (2014) 329–335.
[23] S. Hussain, R.K. Roy, A.K. Pal, Incorporation of silver nanoparticles in DLC matrix and surface plasmon resonance effect, Mater. Chem. Phys. 99 (2006) 375–381.
[24] F.R. Marciano, L.F. Bonetti, R.S. Pessoa, J.S. Marcuzzo, M. Massi, L.V. Santos, V. Trava-Airoldi, The improvement of DLC film lifetime using silver nanoparticles for use on space devices, Diam. Relat. Mater. 17 (2008) 1674–1679.
[25] H.W. Choi, J.H. Choi, K.R. Lee, J.P. Ahn, K.H. Oh, Structure and mechanical properties of Ag-incorporated DLC films prepared by a hybrid ion beam deposition system, Thin Solid Films 516 (2007) 248–251.
[26] S.F. Ahmed, M.W. Moon, K.R. Lee, Effect of silver doping on optical property of diamond like carbon films, Thin Solid Films 517 (2009) 4035–4038.
[27] B. Ghosh, S.C. Ray, R. Espinoza-Gonzalez, R. Villarroel, S.A. Hevia, P. Alvarez-Vega, Surface plasmon effect in electrodeposited diamond-like carbon films for photovoltaic application, Chem. Phys. Lett. 698 (2018) 60–66.
[28] Y.Y. Shen, T. Qi, Y. Qiao, H.J. Hei, Z.Y. He, S.W. Yu, Optical, electrical and microstructural properties of nanocomposite Ag/diamond by Ag ion implantation and subsequent annealing, Vacuum 123 (2016) 160–166.
[29] N. Savvides, Optical-constants and associated functions of metastable diamond-like amorphous-carbon films in the energy range 0.5–7.3 eV, J. Appl. Phys. 59 (1986) 4133–4145.
[30] Y. Lifshitz, G.D. Lempert, E. Grossman, H.J. Scheibe, S. Voellmar, B. Schultrich, A. Breskin, R. Chechik, E. Shefer, D. Bacon, R. Kalish, A. Hoffman, Optical and photoemission studies of DLC films prepared with a systematic variation of the sp^3:sp^2 composition, Diam. Relat. Mater. 6 (1997) 687–693.
[31] Z. Yin, Z. Akkerman, B.X. Yang, F.W. Smith, Optical properties and microstructure of CVD diamond films, Diam. Relat. Mater. 6 (1997) 153–158.
[32] V.V. Sobolev, A.P. Timonov, V.V. Sobolev, Spectra of optical functions and transitions in diamond, Opt. Spectrosc. 88 (2000) 217–221.
[33] A.C. Ferrari, J. Robertson, Interpretation of Raman spectra of disordered and amorphous carbon, Phys. Rev. B 61 (2000) 14095–14107.
[34] S.R. Sails, D.J. Gardiner, M. Bowden, J. Savage, D. Rodway, Monitoring the quality of diamond films using Raman spectra excited at 514.5 nm and 633 nm, Diam. Relat. Mater. 5 (1996) 589–591.
[35] D.S. Knight, W.B. White, Characterization of diamond films by Raman spectroscopy, J. Mater. Res. 4 (1989) 385–393.
[36] S. Michaelson, A. Stacey, J. Orwa, A. Cimmino, S. Prawer, B. Cowie, O. Williams, D. Gruen, A. Hoffman, Bulk and surface thermal stability of ultra nanocrystalline diamond films with 10–30 nm grain size prepared by chemical vapor deposition, J. Appl. Phys. 107 (2010) 093521.
[37] A.C. Ferrari, J. Robertson, Raman signature of bonding and disorder in carbons, in: J.P. Sullivan, J. Robertson, O. Zhou, T.B. Allen, B.F. Coll (Eds.), Amorphous and Nanostructured Carbon, Materials Research Society, Warrendale, 2000, pp. 299–304.
[38] X. Liu, D. Li, X. Sun, Z. Li, H. Song, H. Jiang, Y. Chen, Tunable dipole surface plasmon resonances of silver nanoparticles by cladding dielectric layers, Sci. Rep. (2015) 5.
[39] V.J. Trava-Airoldi, E.J. Corat, A.F.V. Pena, N.F. Leite, V. Baranauskas, M.C. Salvadori, Columnar CVD diamond growth structure on irregular surface substrates, Diam. Relat. Mater. 4 (1995) 1255–1259.
[40] P.W. May, N.L. Allan, M.N.R. Ashfold, J.C. Richley, Y.A. Mankelevich, Simulations of polycrystalline CVD diamond film growth using a simplified Monte Carlo model, Diam. Relat. Mater. 19 (2010) 389–396.
[41] J.E. Butler, A.V. Sumant, The CVD of nanodiamond materials, Chem. Vap. Depos. 14 (2008) 145–160.
[42] A. Pinchuk, G. von Plessen, U. Kreibig, Influence of interband electronic transitions on the optical absorption in metallic nanoparticles, J. Phys. D. Appl. Phys. 37 (2004) 3133.
[43] T.R. Jensen, M.D. Malinsky, C.L. Haynes, R.P. Van Duyne, Nanosphere lithography: tunable localized surface plasmon resonance spectra of silver nanoparticles, J. Phys. Chem. B 104 (2000) 10549–10556.
[44] P.K. Jain, M.A. El-Sayed, Plasmonic coupling in noble metal nanostructures, Chem. Phys. Lett. 487 (2010) 153–164.
[45] K. Baba, R. Hatada, S. Flege, W. Ensinger, Y. Shibata, J. Nakashima, T. Sawase, T. Morimura, Preparation and antibacterial properties of Ag-containing diamond-like carbon films prepared by a combination of magnetron sputtering and plasma source ion implantation, Vacuum 89 (2013) 179–184.
[46] S. Majeed, K. Siraj, S. Naseem, M.F. Khan, M. Irshad, H. Faiz, A. Mahmood, Structural and optical properties of gold-incorporated diamond-like carbon thin films deposited by RF magnetron sputtering, Mater. Res. Express 4 (2017) 8.
[47] S.L. Zou, L.L. Zhao, G.C. Schatz, Extinction spectra of silver nanoparticle arrays, in: N.J. Halas (Ed.), Plasmonics: Metallic Nanostructures and Their Optical Properties, SPIE-Int Soc Optical Engineering, Bellingham, 2003, pp. 174–181.
[48] Y.J. Jiang, S. Pillai, M.A. Green, Re-evaluation of literature values of silver optical constants, Opt. Express 23 (2015) 2133–2144.
[49] Y.J. Jiang, S. Pillai, M.A. Green, Realistic silver optical constants for plasmonics, Sci. Rep. 6 (2016) 7.
[50] S. Webster, Y. Chen, G. Turri, A. Bennett, B. Wickham, M. Bass, Intrinsic and extrinsic absorption of chemical vapor deposition single-crystal diamond from the middle ultraviolet to the far infrared, J. Opt. Soc. Am. B Opt. Phys. 32 (2015) 479–484.
[51] P.K. Jain, W.Y. Huang, M.A. El-Sayed, On the universal scaling behavior of the distance decay of plasmon coupling in metal nanoparticle pairs: a plasmon ruler equation, Nano Lett. 7 (2007) 2080–2088.